A Wide Scan Quasi-Optical Frequency Diplexer

JOHN J. FRATAMICO, JR., MICHAEL J. GANS, AND GERALD J. OWENS

Abstract—A wide scan quasi-optical frequency diplexer is required for certain antenna applications. A waveguide array is a structure which can fill this requirement and also discriminate proximal frequencies. The wide scan characteristics are enhanced by tilting the waveguide axes with respect to the waveguide–free-space interface. A variational analysis of this structure is presented, as well as experimental verification using a *Ku*-band model.

I. Introduction

IN STEERABLE imaging antennas, there is need for a quasi-optical frequency diplexer which can operate over wide angles of incidence [1]. An example of such a scanning spot beam antenna is shown in Fig. 1. Reflectors are used to produce a large image of a small phased array feed. As a result, the small feed array must have an angular field of view M times larger than that required of the overall antenna (where M is the magnification of the reflector arrangement). By placing a quasi-optical frequency diplexer in front of the feed array at an oblique angle to the center ray, it is possible to separate the transmit and receive bands into two separate feed arrays. This allows the feed array designs to be optimized for each frequency band and, compared to diplexer filters in the feed network, the quasi-optical diplexer has lower reflection ripple and transmitter to receiver leakage because reflections from the diplexer and leakage through the diplexer are radiated out into space. However, because of the magnification, the quasi-optical diplexer must operate over a wide range of angles of incidence.

In this paper we describe a waveguide array diplexer which can discriminate proximal frequencies with low sensitivity to incident scan angle. In the process, we solve the problem of scattering from a tilted periodic structure. The particular diplexer described here will pass 14.0–14.5 GHz and reflect 11.7–12.2 GHz with incident scan angles of 40°–60° into the E-plane, and −20°–+20° into the H-plane.

Traditional Fabry–Perot diplexers are unable to operate over such wide scans and still maintain good frequency discrimination. In addition, they exhibit walkoff at large incident angles [2]. This problem is aggravated by using multilayers.

Manuscript received April 30, 1981; revised July 30, 1981.

J. J. Fratimico, Jr., is with Massachusetts Institute of Technology, Cambridge, MA 02139.

M. J. Gans and G. J. Owens are with Bell Laboratories, Crawford Hill Laboratory, Holmdel, NJ 07733.

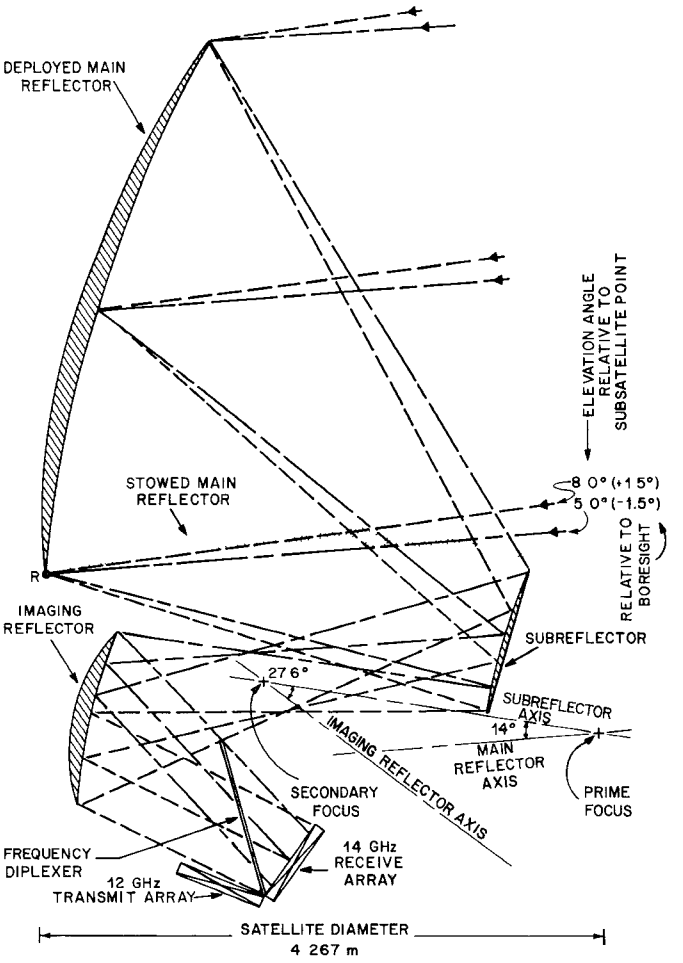

Fig. 1. Imaging satellite antenna with 12/14-GHz frequency diplexing and overall magnification of 7.

Resonant grids have also been used as diplexers. It is possible to design a resonant grid which will behave as a four-pole filter, e.g., the gridded Jerusalem cross [3]. With this arrangement, a single grid may be used to separate frequencies as close as 1.5 : 1.

To separate closer frequencies, there is strong motivation to using a structure with a well-defined cutoff. In this way, arbitrarily large attenuation of the stopband may be obtained by making the structure longer. A periodic array of waveguides is a structure fitting this requirement [4]. The dimensions of the guides and the periodicity of the lattice are parameters with which the filtering properties of the

0018-9480/82/0100-0020$00.75

diplexer may be adjusted. If necessary, iris and dielectric loading can be employed [5].

In fabricating a waveguide array, it is possible to tilt the waveguide axis with respect to the waveguide–free-space interface. It will be shown that significant improvement can be obtained by tilting the axes in the direction of the large angle scan. Motivation for this procedure is derived from analysis of thin, tilted, parallel plates. If the plates are tilted to an angle of θ, then they provide unity transmission to E-plane scans of $\pm\theta$. (The minus sign follows from reciprocity.) Therefore, we expect that a large E-plane tilt will improve diplexer performance by providing less insertion loss throughout the passband over a wider range of incidence angles.

II. Analysis

Since the diplexer is a periodic structure, the tangential components of the scattered fields may be decomposed into Floquet modes [6]. The modes, orthonormalized over a period, are given by

$$\bar{\Psi}_{1pq}=\frac{\exp\left(-j(k_x x+k_y y)\right)}{(d_x d_y)^{1/2}}\left(\frac{k_y}{k_r}\hat{x}-\frac{k_x}{k_r}\hat{y}\right)$$

$$\bar{\Psi}_{2pq}=\frac{\exp\left(-j(k_x x+k_y y)\right)}{(d_x d_y)^{1/2}}\left(\frac{k_x}{k_r}\hat{x}+\frac{k_y}{k_r}\hat{y}\right) \quad (1)$$

where $\bar{\Psi}_{1pq}$ is the (p,q) TE Floquet mode and $\bar{\Psi}_{2pq}$ is the (p,q) TM mode. If (t_x,t_y) are the incident direction cosines, then

$$k_x=k_0 t_x-\frac{2\pi p}{d_x}$$

$$k_y=k_0 t_y-\frac{2\pi q}{d_y}+\frac{2\pi p}{d_x\tan(\alpha)}$$

$$k_r=\left(k_x^2+k_y^2\right)^{1/2} \quad (2)$$

where d_x, d_y, and α are lattice constants, as shown in Fig. 2. The propagation coefficient Γ is given by

$$\Gamma^2=k_r^2-k_0^2. \quad (3)$$

Inside the guides, it is most convenient to use the TE and TM waveguide modes, as these individually satisfy the wall boundary conditions. The tangential components of the electric and magnetic fields for the reference waveguide are given by

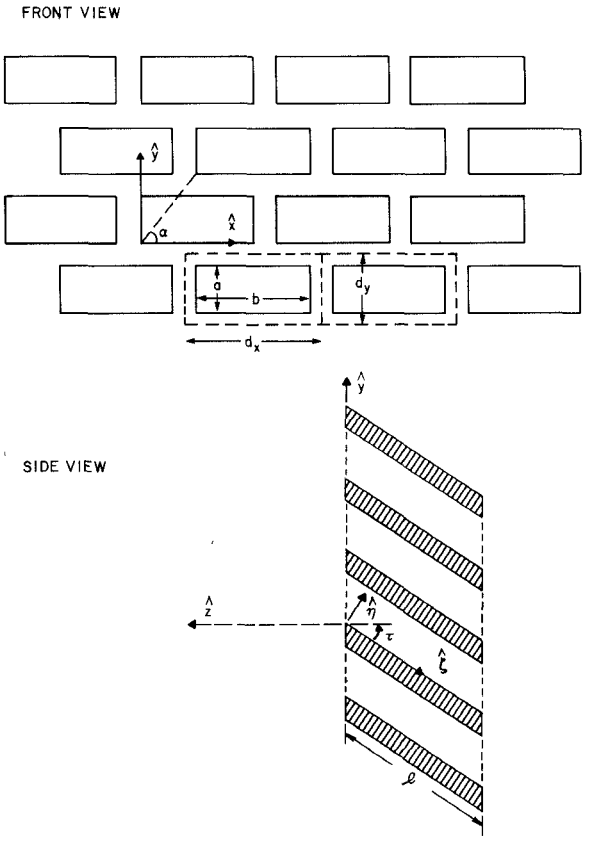

Fig. 2. Waveguide array diplexer. Region C is $d_x\times d_y$ and region A is $a\times b$.

where

$$k_\xi=\frac{m\pi}{b}$$

$$k_\eta=\frac{n\pi}{a\cos\tau}$$

$$k_\rho^2=k_\xi^2+k_\eta^2$$

$$\gamma^2=k_\rho^2-k_0^2. \quad (5)$$

The modes in the other waveguides are phase shifted in such a way as to be consistent with the excitation. Note that the waveguide modes are not orthogonal over the aperture surface. It is not possible in general to choose a set of modes for which both orthogonalization conditions

$$\bar{e}_{1mn}=\exp(\gamma y\sin\tau)\left[-k_\eta\cos k_\xi x\sin\left(k_\eta y\cos\tau\right)\hat{x}+k_\xi\sin k_\xi x\cos\left(k_\eta y\cos\tau\right)\cos\tau\hat{y}\right]$$

$$\hat{z}\times\bar{h}_{1mn}=\exp(\gamma y\sin\tau)\left[\frac{-\gamma}{j\omega\mu_0}k_\eta\cos k_\xi x\sin\left(k_\eta y\cos\tau\right)\cos\tau+\frac{k_\rho^2}{j\omega\mu_0}\cos k_\xi x\cos\left(k_\eta y\cos\tau\right)\sin\tau\right]\hat{x}$$

$$\bar{e}_{2mn}=\exp(\gamma y\sin\tau)\left[-k_\xi\cos k_\xi x\sin\left(k_\eta y\cos\tau\right)\hat{x}-\left[k_\eta\sin k_\xi x\cos\left(k_\eta y\cos\tau\right)\cos\tau+\frac{k_\rho^2}{\gamma}\sin k_\xi x\sin\left(k_\eta y\cos\tau\right)\sin\tau\right]\hat{y}\right]$$

$$\hat{z}\times\bar{h}_{2mn}=\exp(\gamma y\sin\tau)\frac{-j\omega\epsilon_0}{\gamma}\left[k_\xi\cos k_\xi x\sin\left(k_\eta y\cos\tau\right)\cos\tau\hat{x}+k_\eta\sin k_\xi x\cos\left(k_\eta y\cos\tau\right)\hat{y}\right] \quad (4)$$

hold, that is to have simultaneously

$$\int_A d^2r\bar{e}_{rmn}\cdot\bar{e}^*_{r'pq}\propto\delta_{rmn,r'pq}$$

$$\int_A d^2r\bar{e}_{rmn}\cdot\hat{z}\times\bar{h}^*_{r'pq}\propto\delta_{rmn,r'pq}. \tag{6}$$

We first determine the scattering matrix for a semi-infinite diplexer. Suppose the incident field is from free space ($z>0$). Then, replacing triple subscripts by single subscripts

$$\bar{E}=\bar{E}^{inc}+\sum_i V_i\bar{\Psi}_i=\sum_i a_i\bar{e}_i \quad \mathbb{R}(C) \tag{7}$$

$$\hat{z}\times\bar{H}=\hat{z}\times\bar{H}^{inc}-\sum_i Y_iV_i\bar{\Psi}_i=\sum_i a_i\hat{z}\times\bar{h}_i \quad \mathbb{R}(A) \tag{8}$$

where (Y_i) is the modal admittance of the ith Floquet mode

$$Y_i=\begin{cases}\dfrac{\Gamma_i}{j\omega\mu_0}, & \text{TE}\\[2ex] \dfrac{j\omega\epsilon_0}{\Gamma_i}, & \text{TM.}\end{cases} \tag{9}$$

Exploiting the orthonormality of $\bar{\Psi}$, we obtain

$$2\hat{z}\times\bar{H}^{inc}=\int_C d^2r'\left[\sum_i Y_i\bar{\Psi}_i(r)\bar{\Psi}^*_i(r')\right]\cdot\left[\sum_j a_j\bar{e}_j(r')\right]+\sum_i a_i\hat{z}\times\bar{h}_i(r). \tag{10}$$

Taking the inner product with $(\bar{e}^*_l)$ and defining

$$D_{lm}\triangleq\int_A d^2r\bar{e}_l(r)\cdot\hat{z}\times\bar{h}^*_m(r)$$

$$F_{lm}\triangleq\int_A d^2r\bar{e}_l(r)\cdot\bar{\Psi}^*_m(r) \tag{11}$$

we obtain

$$2\int_A d^2r\bar{e}^*_l\cdot\hat{z}\times\bar{H}^{inc}=\sum_{i,j}\left(Y_iF^*_{li}F_{ji}+D^*_{lj}\delta_{ij}\right)a_j. \tag{12}$$

This equation is solved for the a_j by means of a matrix inversion. The V_j are determined by continuity of electric field

$$V_j=\sum_i a_iF_{ij}-\int_{\hat{C}} d^2r\bar{E}^{inc}\cdot\bar{\Psi}^*_j. \tag{13}$$

Thus we have determined the scattered field for arbitrary free-space excitation. It can be shown that this analysis is variational in the assumed aperture field [7]. It also has the desirable property of conserving complex Poynting power across the aperture.

To completely specify the scattering matrix, we must also consider the problem of scattering from a waveguide

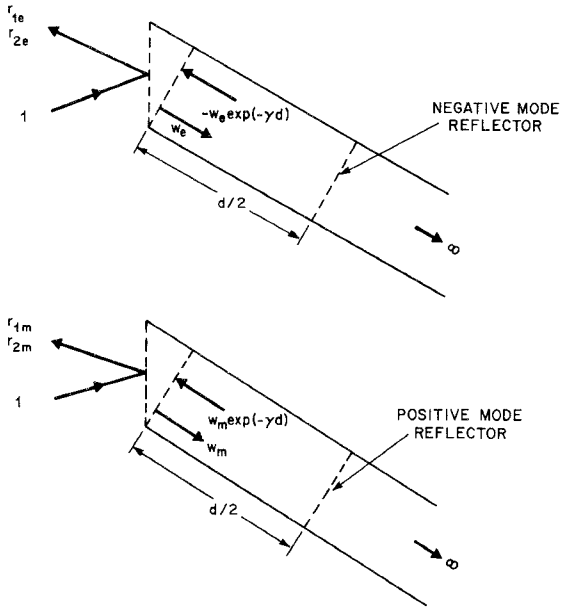

Fig. 3. Inserted currents. Negative mode reflector is an electric current wall; positive mode reflector is a magnetic current wall.

incident mode. Direct solution is complicated by the non-orthogonality of the waveguide modes, and fails to achieve the variational and power conserving properties listed above. An indirect solution is obtained by resolving the free-space incidence problem in the presence of a waveguide scatterer. (Fig. 3.) The scatterer may be chosen in such a way that it supports those currents, electric or magnetic, which will reflect only one waveguide mode. The reflection coefficient will be chosen either plus or minus one for that particular mode, but will be zero for all other modes. Therefore we calculate the scattered fields twice, once in the presence of a positive waveguide mode reflector, and once with a negative reflector. By combining the results of these calculations, the relevant scattering coefficients for a given waveguide mode may be determined.

The presence of these single mode scatterers affects the analysis in a trivial way. For instance, suppose we are interested in scattering from the TE_{10} mode. Then the dominant mode fields at the aperture become

$$\begin{aligned}\bar{e}_{110}&=\frac{\pi}{b}\sin\left(\frac{\pi x}{b}\right)\\&\quad\cdot\cos\tau\left[\exp\left(\gamma_{10}y\sin\tau\right)\mp\exp\left(-\gamma_{10}d-\gamma_{10}y\sin\tau\right)\right]\hat{y}\\ \hat{z}\times\bar{h}_{110}&=\hat{x}\left(\frac{\pi}{b}\right)^2\frac{1}{j\omega\mu_0}\cos\left(\frac{\pi x}{b}\right)\\&\quad\cdot\sin\tau\left[\exp\left(\gamma_{10}y\sin\tau\right)\mp\exp\left(-\gamma_{10}d-\gamma_{10}y\sin\tau\right)\right]\\&\quad+\hat{y}\frac{\gamma_{10}}{j\omega\mu_0}\frac{\pi}{b}\sin\frac{\pi x}{b}\\&\quad\cdot\left[\exp\left(\gamma_{10}y\sin\tau\right)\pm\exp\left(-\gamma_{10}d-\gamma_{10}y\sin\tau\right)\right]\end{aligned} \tag{14}$$

where the lower signs indicate positive reflection, and the upper signs indicate negative reflection. We can then combine the solutions to obtain the scattered fields from free space or waveguide incidence (Figs. 4 and 5).

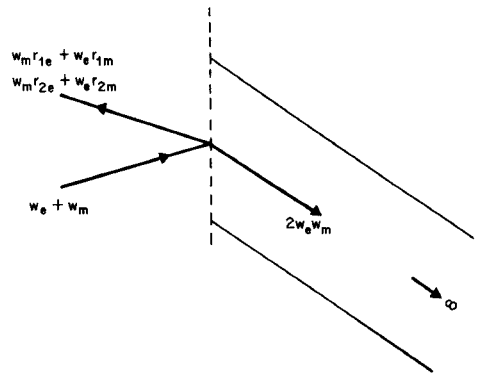

Fig. 4. Free-space incidence. No reflected wave inside the guide.

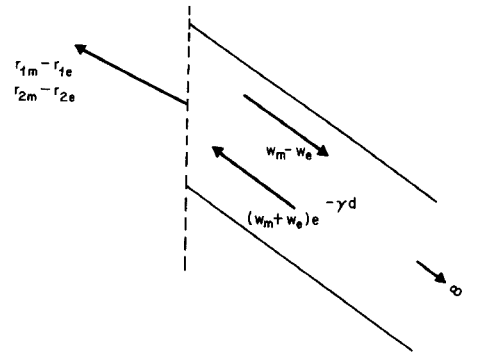

Fig. 5. Waveguide incidence. No reflected wave in free space.

Since a magnetic wall will produce a positive reflection, and an electric wall will produce a negative reflection, we denote by subscript m the fields scattered with a positive reflector, and by e the fields scattered with a negative reflector, as indicated in Fig. 3. Letting sub w represent the waveguide mode of interest, and subs 1 and 2 the copolarized and cross-polarized free-space modes, respectively, we obtain the scattering coefficients

$$S_{11} = \frac{w_m r_{1e} + w_e r_{1m}}{w_m + w_e}$$

$$S_{21} = \frac{w_m r_{2e} + w_e r_{2m}}{w_m + w_e}$$

$$S_{w1} = \frac{2w_m w_e}{w_m + w_e}$$

$$S_{ww} = \frac{w_m - w_e}{w_m + w_e} \exp(-\gamma_{10} d)$$

$$S_{1w} = \frac{r_{1m} - r_{1e}}{w_m + w_e} \exp(-\gamma_{10} d)$$

$$S_{2w} = \frac{r_{2m} - r_{2e}}{w_m + w_e} \exp(-\gamma_{10} d). \tag{15}$$

The scattering matrix for the apertures on the other side of the diplexer are found in the same way. Note that symmetry requires that conjugate excitation be considered on the opposite side. Once the scattering matrices for the apertures are calculated, it is a straightforward procedure to calculate overall transmission. In a practical design, only the dominant mode appreciably couples the apertures. Under this condition, we have

$$T_{copol} = \frac{S^l_{w1} S^r_{1w} \exp(-\gamma_{10} l_e)}{1 - S^r_{ww} S^l_{ww} \exp(-2\gamma_{10} l_e)}$$

$$R_{copol} = S^l_{11} + \frac{S^l_{w1} S^l_{1w} S^r_{ww} \exp(-2\gamma_{10} l_e)}{1 - S^r_{ww} S^l_{ww} \exp(-2\gamma_{10} l_e)}$$

$$T_{xpol} = \frac{S^l_{w1} S^r_{2w} \exp(-\gamma_{10} l_e)}{1 - S^r_{ww} S^l_{ww} \exp(-2\gamma_{10} l_e)}$$

$$R_{xpol} = S^l_{21} + \frac{S^l_{w1} S^l_{2w} S^r_{ww} \exp(-2\gamma_{01} l_e)}{1 - S^r_{ww} S^l_{ww} \exp(-2\gamma_{01} l_e)} \tag{16}$$

where superscript l indicates the scattering coefficient from the aperture on the incident side of the diplexer, and superscript r indicates the scattering coefficient from the opposite side. The length between reference planes l_e is given by

$$l_e = l - a \sin\tau. \tag{17}$$

III. Accuracy of Analysis

The accuracy of this calculation is greatly supported by the variational nature of the analysis; i.e., the scattering coefficients are stationary in the assumed aperture fields. Since the aperture electric field is approximated by a sum over the waveguide modes, we require only a small number of waveguide modes to yield accurate scattering parameters. This is fortunate, as the size of the matrix to be inverted is equal to the number of such modes used. Satisfactory convergence was obtained using 10 waveguide modes and 98 Floquet modes (all Floquet modes with indices ≤ 3). Note that the Floquet modes affect a summation rather than an inversion.

It is useful to check the numerical accuracy of the program, in particular the matrix inversion. This may be done by calculating the approximate complex Poynting power on either side of an aperture. The analysis guarantees that this quantity should be continuous, even when the number of modes is truncated. An advantage was found in using a double precision inversion routine, as the matrix was not always well tempered.

In addition, there exist sets of conditions under which the structure becomes an analytically solvable scattering problem. When the diplexer is a block array of infinitesimally thin walls, and the excitation is from the H- or quasi-E-planes, the scattering problem becomes scalar, and can be solved by the Wiener–Hopf technique [8]. Such an analysis was performed, and there was found to be excellent agreement.

IV. Results

An important consideration in periodic scattering is the elimination of grating lobes. The incipience of grating lobe propagation is marked by a discontinuity in the first derivative of the transmission coefficient, and a significant misdirection of power.

From (2), (3), the conditions for grating lobe elimination are apparent. The (p, q) mode will be evanescent when

$$\left(k_x^2+k_y^2\right)_{p,q}>k_0^2. \tag{18}$$

For a block array ($\alpha=90°$), grating lobes will be eliminated if

$$\max\left(t_y\right)<\frac{2\pi}{k_0 d_y}-1 \tag{19a}$$

$$\max\left(t_x\right)<\frac{2\pi}{k_0 d_x}-1. \tag{19b}$$

Condition (19a) is easily satisfied, as $(k_0 d_y)$ may be made arbitrarily small. However, condition (19b) is an important constraint, as $(k_0 d_x)$ must be greater than π at the low end of the passband. This suggests the inappropriateness of placing the large angle scan in the H-plane.

The situation is improved by using a brick structure $\left(\alpha=\arctan\left(2d_y/d_x\right)\right)$. If $\left(\pi/2k_0 d_y\right)$ is made larger than unity, the only constraint becomes

$$\max\left(t_x\right)<\frac{4\pi}{k_0 d_x}-1. \tag{20}$$

This condition is easily satisfied for all incident scans.

The higher order modes, even when evanescent, represent a reactive load of the scatterer. Their dependence on frequency and incidence angle is minimized by making (k_r) as large as possible. This is motivation for choosing a brick array with high aspect ratio waveguides.

The various parameters of the diplexer were varied so as to provide, for a range of scan angles from 37.5°–62.5° into the E-plane and −22.5–22.5° into the H-plane, the least insertion loss over the receive frequency band (passband) while maintaining no more than 0.2 dB return loss in the transmit frequency band (stopband). Results were relatively insensitive to H-plane wall thickness, so it was chosen thick enough for strength. The E-plane waveguide height was chosen as large as possible, without significant reduction in diplexer performance, to reduce fabrication cost. In this way an optimum design was determined with computed results. The results indicated the following optimum diplexer properties: the width of the waveguides is determined by cutoff frequency, which must lie between the two bands. The length of the guides corresponds to approximately one half of a guide wavelength in the passband. Best wide scan performance is obtained when the tilt angle is chosen close to the larger E-plane scan. The E-plane wall thickness cannot be too thick *or* too thin without degrading the electrical properties.

For application to the scanning spot beam antenna, the optimal design was numerically found to be

$b=1.16$ cm, brick array
$a=0.22$
$d_x=1.26$
$d_y=0.32$
$l=2.40$

and

$\tau=0.95$ rad.

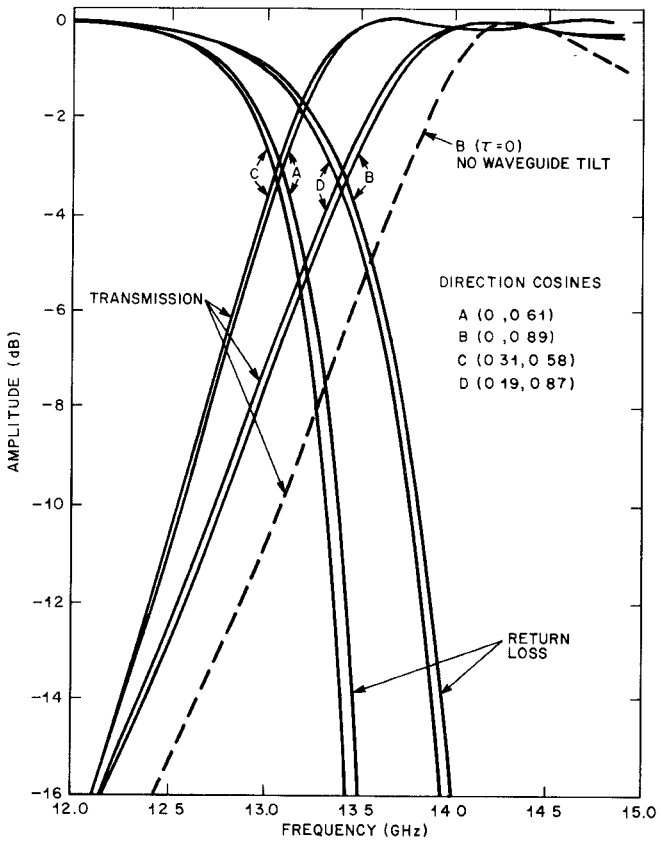

Fig. 6. Optimal diplexer transmissivity. This diplexer employs a brick array, $\tan\alpha=2d_y/d_x$.

As shown in Fig. (6), the diplexer produces a coupling loss of less than 0.3 dB in the passband, and a return loss of no more than 0.2 dB in the stopband. The phase of the transmitted field is nearly flat across the passband.

For comparison, the dashed curve in Fig. 6 shows the transmission at 62.5° E-plane scan of an optimized diplexer with zero waveguide tilt (whose dimensions were found to be identical to the tilted guide diplexer, except $\tau=0$). Note that the passband is much narrower.

V. Experiment

An experiment was performed to further verify the analysis presented in this paper. The diplexer which was built is described by the following parameters (see Fig. 7)

$b=1.168$ cm, block structure
$a=0.509$
$d_x=1.270$
$d_y=0.686$
$l=2.388$
$\tau=0.96$ rad.

This suboptimal design (block rather than brick and reduced aspect ratio) was chosen to expedite fabrication. The overall dimensions of the diplexer are 79 cm (E-plane) by 38 cm (H-plane). The dimensions were chosen so that the projection would be approximately square when viewed from a 60° E-plane scan.

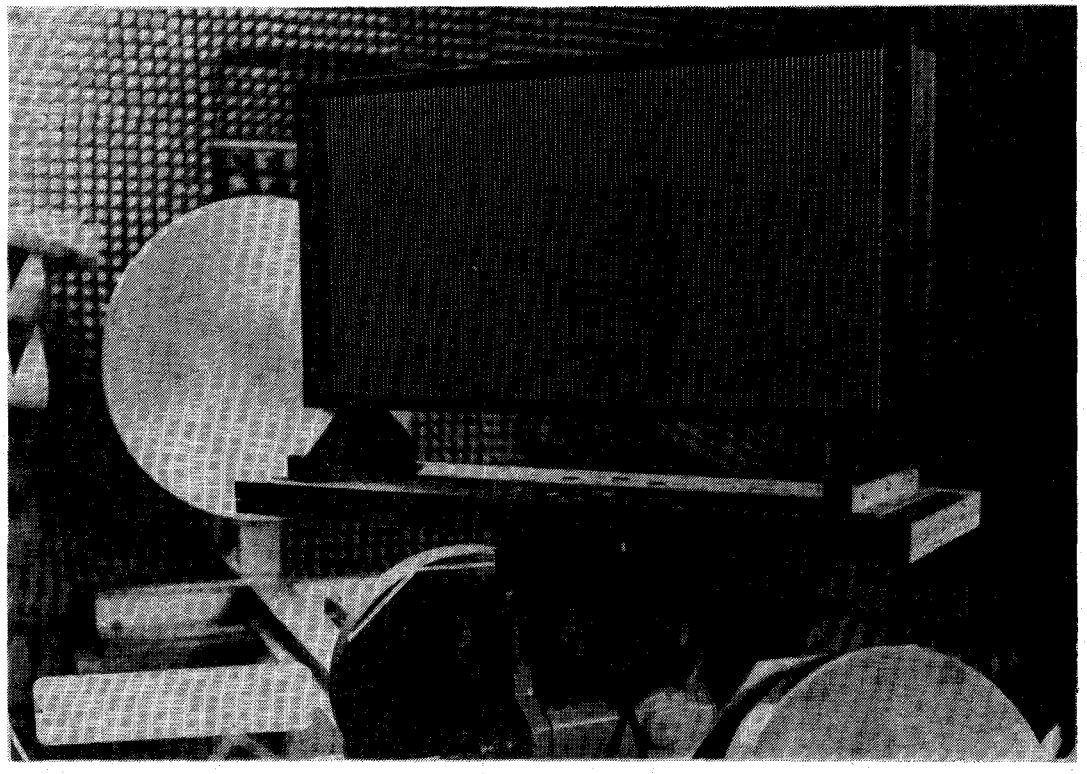

Fig. 7. Experimental diplexer using egg-crate block construction.

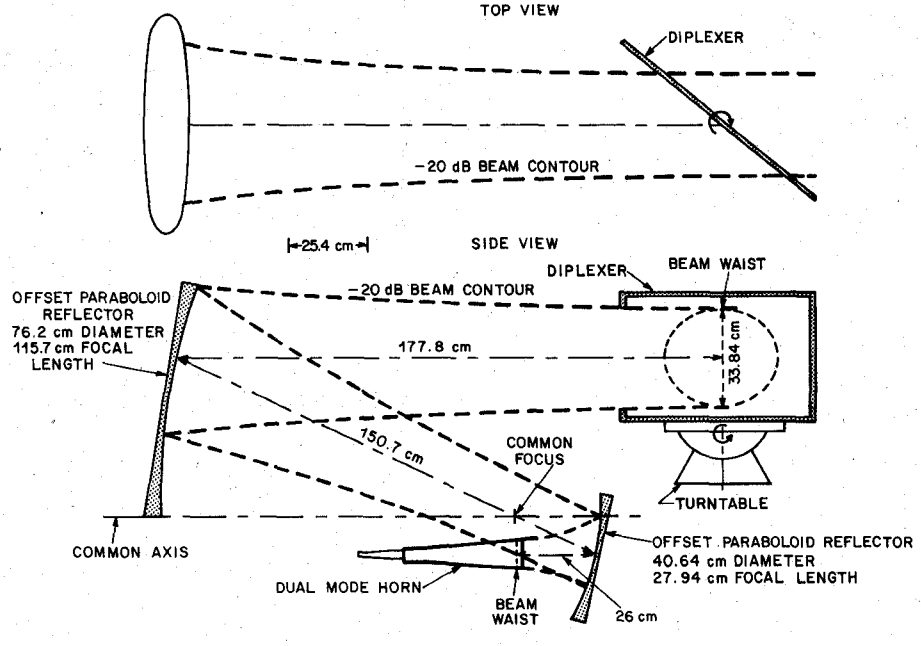

Fig. 8. Gaussian beam design for measuring the diplexer.

The transmissivity of the diplexer was determined by an insertion loss measurement. Two launchers were used to form a symmetric focused Gaussian system. The reduction in coupling caused by placing the diplexer at the beam waist provided a measure of transmission loss. The beam size was chosen such that the −20-dB part of the beam was near the perimeter of the diplexer. At 14 GHz, the Gaussian beam had an angle spread of approximately ±2.5° to the −20-dB points.

The data was taken by sweeping in frequency. It was therefore important that the location of the beam waist be frequency independent. A single reflector launcher cannot achieve this property. However, it is easily shown that a dual reflector confocal launcher does transform a source to an image, independent of frequency. To minimize blockage, an offset confocal arrangement was used, as shown in Fig. 8. Only one of the two beam launchers is shown. An identical launcher is placed on the far side of the diplexer

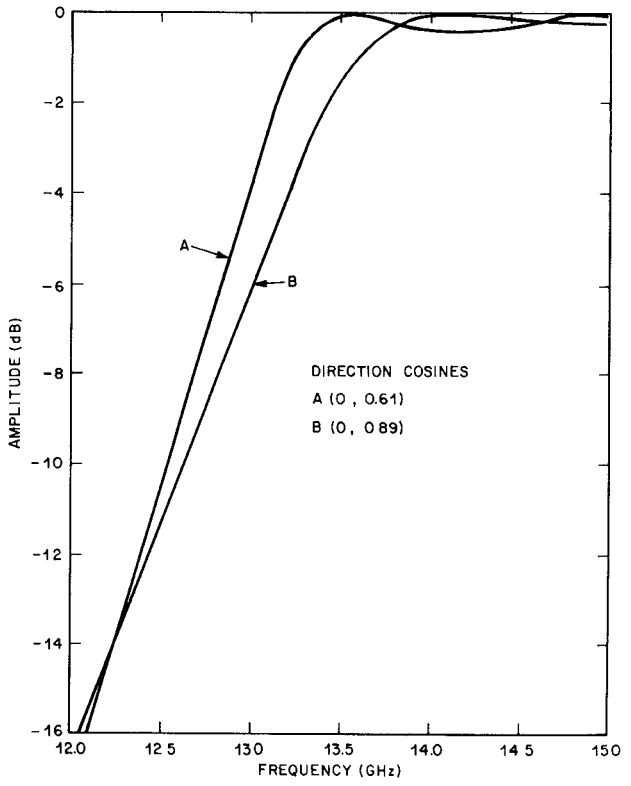

Fig. 9. Calculated transmission at extreme incidence angles.

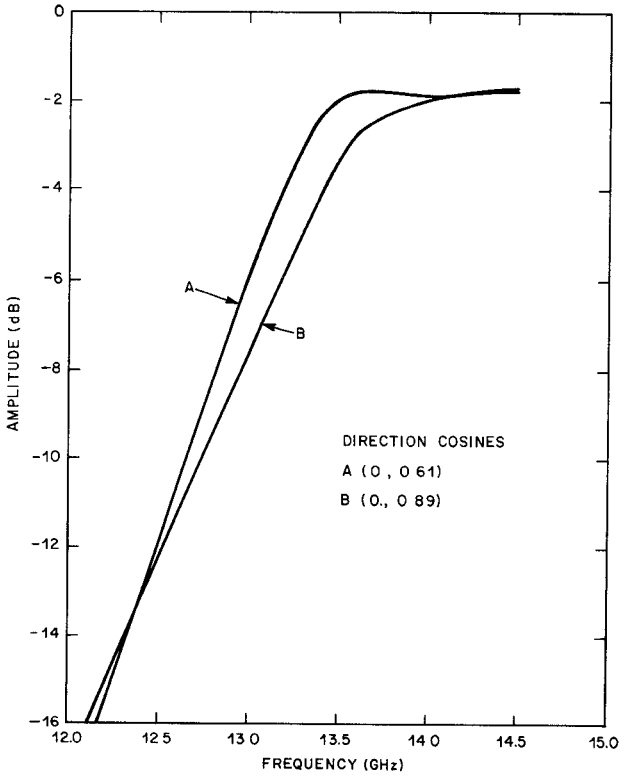

Fig. 10. Measured transmission corresponding to calculated curves of Fig. 9.

for transmission measurements and in the specular reflection direction for reflection measurements. Reflection measurements were compared to a flat conducting plate.

The feeds selected were dual mode horns [9]. These conical horns combine the TE_{11}^0 and TM_{11}^0 modes in such a way as to obtain a nearly symmetric radiation pattern, coincident phase centers in the principal planes, and well suppressed side lobes.

The theoretical and experimental results are shown in Figs. 9 and 10. We note that the frequency behavior of the two plots are in close agreement. Also, the measured transmissivity was insensitive to small H-plane scans, as predicted (result not shown). However, the experimental curve shows an additional 2-dB insertion loss. Further experiments indicate that the reflected power could account for no more than 0.5 dB of this loss. Therefore, we conclude that most of the disparity is due to ohmic dissipation. This is probably due to the method of diplexer fabrication, an "egg crate" technique. Slits were made in the horizontal and vertical vanes in such a way that they could slide together. This unfortunately leaves gaps in the corners of the waveguides, where dominant mode current is at a maximum. To overcome this problem, the diplexer was coated with a silver conducting paint several skin depths in thickness. Since the paint resistivity is much greater than that of metal, we experience absorption loss. It is expected that this loss could be significantly reduced by dipping the diplexer into a metal bath.

By rotating the diplexer during reflection, negligible beam broadening was observed relative to the flat plate and side lobe variations relative to the flat plate indicate scattering in directions other than specular were at least 40 dB lower than in the specular direction.

VI. Conclusion

It is demonstrated in this paper that a waveguide array diplexer can meet the severe specifications imposed by a steerable imaging antenna. Its frequency dependence is largely geometric, and therefore it is relatively insensitive to incident scanning angle. It does not rely on exciting a resonance to reflect the stopband, and therefore its return loss is not as sensitive to ohmic dissipation as a resonant grid.

The analysis of this structure takes into account waveguide dimensions, lattice dimensions, tilt angle, and incident scan angle. It does not consider the effects of loss, although a perturbative modification would not be difficult. An interesting feature of the analysis is that it provides variational, power conserving expressions for scattering from a tilted interface. Waveguide mode orthogonalization was not required to produce these properties.

Acknowledgment

The authors are pleased to acknowledge C. Dragone and A. A. M. Saleh for many helpful discussions and G. Kodym and A. Quigley for construction of the tilted vane diplexer.

References

[1] C. Dragone and M. J. Gans, "Imaging reflector arrangements to form a scanning beam using a small array," *Bell Syst. Tech. J.*, vol. 58, no. 2, pp. 501–515, 1979.

[2] J. A. Arnaud, A. A. M. Saleh, and J. T. Ruscio, "Walk-off effects in Fabry–Perot diplexers," *IEEE Trans. Microwave Theory Tech.*, vol.

MTT-22, pp. 486–493, May 1974.
[3] J. A. Arnaud and F. A. Pelow, "Resonant grid quasi-optical diplexers," *Bell Syst. Tech. J.*, vol. 54, no. 2, pp. 263–283, 1975.
[4] C. C. Chen, "Transmission of microwaves through perforated flat plates of finite thickness," *IEEE Trans. Microwave Theory Tech.*, vol. MTT-21, pp. 1–6, Jan. 1973.
[5] R. J. Luebbers and B. A. Munk, "Some effects of dielectric loading on periodic slot arrays," *IEEE Trans. Antennas Propagat.*, vol. AP-26, pp. 536–542, Apr. 1978.
[6] N. Ammitay, V. Galindo, and C. P. Wu, *Theory and Analysis of Phased Array Antennas*. New York: Wiley, 1972.
[7] J. J. Fratamico, "A wide scan quasi-optical frequency diplexer," S.M. thesis, Massachusetts Institute of Technology, Cambridge, MA, 1980.
[8] J. F. Carlson and A. Heins, "The reflection of an electromagnetic plane wave by an infinite set of plates," *Quart. Appl. Math.*, 4, no. 4, pp. 313–329, 1947.
[9] P. D. Potter, "A new horn antenna with suppressed sidelobes and equal beamwidths," *Microwave J.*, vol. 6, pp. 71–78, 1963.

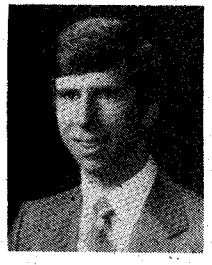

John J. Fratamico, Jr. was born in Glens Falls, NY on March 6, 1957. He received the S.B., S.M., and Eng. degrees in electrical engineering in 1980, 1980, and 1981, respectively, all from the Massachusetts Institute of Technology, Cambridge.

He is presently working toward his doctorate at M.I.T., with fellowship support from the Fannie and John Hertz Foundation. His current research interests include the design of curved dichroic surfaces, and the propagation of millimeter waves through a turbid atmosphere.

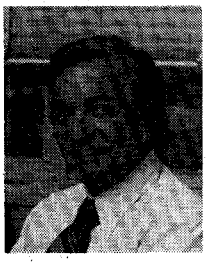

Michael J. Gans received the B.S. degree in electrical engineering from Notre Dame University, South Bend, IN, in 1957, and the M.S. and Ph.D. degrees in electrical engineering from the University of California, Berkeley, in 1961 and 1965, respectively.

At Bell Laboratories, he has been engaged in research on antennas for mobile radio and satellite communications.

Gerald J. Owens served in the U.S. Navy from 1950 to 1954. He joined Bell Laboratories, Holmdel, NJ, in 1955. He was associated with various military radar projects, the earth station tracking receivers for the Telstar project, solar radio telescopes, and, more recently, computer controlled voice response systems. He is currently engaged in research on satellite antennas.

Numerical Evaluation of Lumped Inductance Influences of Superconducting Circuit Interconnections on Ultrafast Switching Signal Propagation Characteristics

JIRO TEMMYO AND HARUO YOSHIKIYO

Abstract—**The lumped inductance influences of superconducting circuit interconnections on ultrafast switching (~10 ps) signal propagation characteristics, such as propagation delay, degraded switching time, reflections, amplitude distortions, and crosstalk, were for the first time quantitavely evaluated by using the LNAP computer simulation, including the influences of matching capacitors and terminated resistor value.**

Manuscript received February 27, 1981; revised August 18, 1981.

The authors are with the Musashino Electrical Communication Laboratory, Nippon Telegraph and Telephone Public Corporation, 3-9-11, Midoricho, Musashino-shi, 180 Tokyo, Japan.

I. INTRODUCTION

JOSEPHSON LOGIC and memory chips are being investigated to evaluate its potential for high performance computers [1]. The very low power dissipation of Josephson chips permits its high circuit density per unit

0018-9480/82/0001-0027$00.75 ©1982 IEEE